Eur Biophys J (2011) 40:1071–1079
DOI 10.1007/s00249-011-0724-1

ORIGINAL PAPER

Force–velocity relationship for multiple kinesin motors pulling a magnetic bead

Todd L. Fallesen · Jed C. Macosko · G. Holzwarth

Received: 30 January 2011 / Revised: 7 June 2011 / Accepted: 12 June 2011 / Published online: 7 July 2011

Abstract Although the velocity of single kinesin motors against an opposing force F of 0–10 pN is well known, the behavior of multiple kinesin motors working to overcome a larger load is still poorly understood. We have carried out gliding assays in which 3–7 *Drosophila* kinesin-1 motors moved a microtubule at 200–700 μm/s against a 0–31 pN load at saturating [ATP]. The load F was generated by applying a spatially uniform magnetic field gradient to a superparamagnetic bead attached to the (+) end of the microtubule. When F was scaled by the average number of motors $\langle n \rangle$, the force–velocity relationship for multiple motors was similar to the force–velocity relationship for a single motor, supporting a minimal load-sharing model. The velocity distribution at low load has a single mode consistent with rapid fluctuations of n. However, against a load of 2.5–4.7 pN/motor, additional modes appeared at lower velocity. These observations support the Klumpp–Lipowsky model of multimotor transport [Proc Natl Acad Sci USA 102. 17284–17289 (2005)].

Keywords Motor protein · Motility assay · Kinesin · Magnetic bead · Multiple motor

Abbreviations

SEM	Standard error of the mean
BRB80	Brinkley reconstitution buffer

T. L. Fallesen · J. C. Macosko · G. Holzwarth (✉)
Department of Physics, Wake Forest University, PO Box 7507, Winston-Salem, NC 27109, USA
e-mail: gholz@wfu.edu

Introduction

Kinesin-1 is a processive dimeric motor protein which moves along microtubules at average velocity of 600–800 nm/s (Visscher et al. 1999). It consists of two identical heavy chains, each containing 960–1,030 amino acids (Hirokawa et al. 2009). Motors move along the microtubule in a series of 8-nm "hand-over-hand" steps, hydrolyzing one adenosine triphosphate (ATP) per step (Coy et al. 1999; Nan et al. 2008; Watanabe and Higuchi 2007; Yildiz et al. 2004).

The velocity for a single kinesin has been measured against an opposing force generated by an optical trap, a glass needle, and viscous drag (Hunt et al. 1994; Meyhöfer and Howard 1995; Visscher et al. 1999). The average velocity decreases as the opposing force increases until the motor stalls against a force of 5–7 pN (Coppin et al. 1997; Kojima et al. 1997; Visscher et al. 1999). The shape of the force–velocity curve is usefully described by the three-parameter relationship (Kunwar and Mogilner 2010),

$$v = v_0\left(1 - \left[F/F_s\right]^w\right), \tag{1}$$

where the zero-force velocity $v_0 \approx$ 650–800 nm/s and the stall force $F_s =$ 4–8 pN (Howard 2001). The parameter w is called the curvature index. When $w = 1$, Eq. 1 is linear. For $w < 1$, $d^2v/dF^2 > 0$ and all values of v lie below the straight line. For $w > 1$, $d^2v/dF^2 < 0$ and all values of v lie above the straight line. If we fit Eq. 1 to published data for kinesin-1 from bovine brain (Hunt et al. 1994) and squid (Visscher et al. 1999), we find that w equals 1 and 2.5, respectively.

In contrast to the situation for single motors, the collective dynamics of two or more kinesin motors pulling a microtubule, bead, vesicle or other cargo is

poorly understood. In microtubule gliding assays, the velocity of the cargo is independent of the surface density of motors if the surface density is less than $\sim$5,000 μm^{-2} and the opposing force is less than 0.1 pN (Gibbons et al. 2001; Howard et al. 1989). However, if the surface density exceeds 5,000 μm^{-2}, the velocity in the absence of load decreases with increasing number of motors, presumably due to interference by crowding (Bieling et al. 2008).

Cargo transported by multiple motors travels further along a microtubule before falling off than cargo pulled by a single motor (Block et al. 1990; Howard et al. 1989). Also, the stall force for two motors is approximately twice the stall force of a single motor (Vershinin et al. 2007; Welte et al. 1998). These observations invite the question of how the velocity of a cargo pulled by multiple motors changes in response to opposing forces greater than 0.1 pN but less than the stall force.

In vivo studies of vesicle transport in cells conflict on whether similar motors pulling a single cargo cooperate or interfere. On the one hand, kinesin-driven lipid droplets in *Drosophila* show a decrease in velocity when the motor number increases from one to two (Shubeita et al. 2008). On the other hand, measurements of the distribution of velocities for vesicles of different sizes in NT2 cells suggest that small numbers of motors cooperate constructively (Shtridelman et al. 2009). Gliding assays through a viscoelastic medium show a similar result: increasing the number of kinesin motors increases the velocity in a manner one would expect if the opposing force is shared between motors (Gagliano et al. 2010).

A central experimental problem in determining reliable force–velocity curves for a cargo driven by multiple motors is establishing how many motors are pulling a given load. To address this difficulty, Jamison et al. (2010) synthesized constructs in which two truncated kinesin motors are linked at their tail ends to opposite ends of a 50-nm DNA duplex. Without an opposing load the average velocity of the two-kinesin construct is the same as the construct with only one motor, but run lengths for two-motor constructs are shorter than would be expected for two independently binding and unbinding motors, suggesting that, at 50 nm separation, the motors in this construct interfere with each other. Against a small force, constructs with two motors tend to transport their cargo using one load-bearing motor at a time. Only for large forces are both motors engaged.

Despite the sparsity of experimental data for multiple-motor effects, several models of multiple-motor dynamics have been published. A dynamical multimotor model of the microtubule gliding assay in buffer (Gibbons et al. 2001) gives a velocity that is independent of the number of motors, in agreement with experiment in buffer (Howard et al. 1989). This independence occurs because the drag force on the moving microtubule in buffer is less than 0.1 pN, which is small compared with the force required to appreciably slow even a single motor.

The bead transport model of Klumpp and Lipowsky (2005) provides a helpful framework for understanding possible multiple-motor interactions in bead or vesicle assays in the presence of significant load. The model assumes that all bound motors share the load equally, but that the number of active motors fluctuates on a timescale of seconds as motors bind and unbind from the microtubule. This model predicts a nonlinear force–velocity curve with $w > 1$ when multiple motors pull a bead against significant force.

A stochastic computer simulation by Korn et al. (2009) extends the Klumpp–Lipowsky model by allowing unequal sharing of the load and by considering hydrodynamic interactions between the moving bead and the stationary surface. This model predicts that bead velocity increases with the number of motors in the presence of significant viscous drag on the bead. This agrees well with our recent measurements on gliding microtubules in a viscous medium (Gagliano et al. 2010).

In this report, we apply a calibrated magnetic force to superparamagnetic beads attached by a biotin–streptavidin linkage to the (+) end of microtubules in a gliding assay. The average number of active motors is 3–7, and the magnetic force is 4–31 pN. Thus, the largest force is about five times the stall force of a single motor. We find that a microtubule with multiple motors continues to glide in the presence of opposing magnetic force, but at a lesser average velocity. The average number of motors propelling the microtubule is evaluated from its length and the average distance between motors, determined experimentally (Fallesen et al. 2011).

Materials and methods

Kinesin

Full-length *Drosophila* kinesin-1 was prepared by *Escherichia coli* transformed with plasmid pPK113 and purified by Ni–NTA chromatography as described by Coy et al. (1999). This plasmid encodes a 987-aa chain, including the 6xhis tag [http://www.ncbi.nlm.nih.gov/protein/AAD13351.1]. Using A_{280} with $\varepsilon_{280} = 42{,}915\ M^{-1}cm^{-1}$, the concentration of the purified kinesin dimer was determined to be 94 μg/mL. Sodium dodecyl sulfate polyacrylamide gel electrophoresis (SDS–PAGE) of the purified protein showed a single band at 115 ± 5 kDa, the molecular weight of kinesin-1 monomer. After purification, the kinesin was snap-frozen in liquid nitrogen and stored at −80°C.

Microtubules

Microtubules were prepared in two steps. First, rhodamine-labeled and unlabeled bovine tubulins (Cytoskeleton, Denver, CO) were copolymerized at ratio of 1:6 by warming to 37°C for 45 min in BRB80 [80 mM piperazine-*N*,*N*′-bis(2-ethanesulfonic acid) (PIPES) buffer, 1 mM ethylene glycol tetraacetic acid (EGTA), 1 mM $MgCl_2$, pH 6.9] supplemented with 1 mM guanosine triphosphate (GTP) and 1 mM dithiothreitol. The resultant fluorescent microtubules were then sheared once through the 26-gauge needle of a 50-µL glass syringe to create shorter microtubules. Biotin-labeled bovine tubulin (Cytoskeleton) was added to the sheared microtubules and heated at 37°C in the presence of GTP for an additional 15 min. The biotin-labeled tubulin polymerized predominantly at the (+) ends of the microtubules. This resulted in the addition of short biotin-labeled tails to the fluorescent microtubules. Small amounts of unpolymerized fluorescent tubulin remained in solution from the first step, causing dim fluorescence of the biotin-labeled tails.

Gliding assays with retarding force parallel to microtubule axis

Upside-down gliding assays (Fig. 1) were done in rectangular glass capillary tubes, 0.05 mm high × 0.5 mm wide × 25 mm long, with interior volume 0.625 µL (Vitrocom, Mountain Lakes, NJ). BRB80 augmented with 0.5 mg/mL casein (Fisher, Atlanta GA) was flowed into the capillary tube and allowed to adsorb for 5 min.

Next, a solution of BRB80 supplemented with 0.2 mg/mL casein, 1 mM Mg-ATP, and 1.5–8.4 µg/mL kinesin was flowed into the tube. Following adsorption of the kinesin molecules to the casein-coated surfaces of the tube (Vale et al. 1992), a solution containing BRB80, 1 mM Mg-ATP, 30 µM taxol, 5 mM $MgCl_2$, microtubules, antifade (40 mM D-glucose, 0.02 mg/mL catalase, 0.04 mg/mL glucose oxidase, 60 mM β-mercaptoethanol), and 0.0375% streptavidin-coated, 2.8-µm-diameter polystyrene superparamagnetic beads (M270; Dynal/Invitrogen, Carlsbad, CA) was flowed into the capillary. Most of the beads became attached to the biotin-labeled tails of microtubules. The ends of the capillary were sealed with biologically inert grease (Mobil FM102; Exxon-Mobil, Houston, TX). The capillary tube was placed into the gap between the pole pieces of an electromagnet in a Nikon Eclipse 6000FN microscope. The pole pieces of the electromagnet were shaped to provide a uniform magnetic force on the beads over a 6 mm length of the capillary tube. The electromagnet took the place of the standard microscope stage, and was used to apply a 4–16 pN force to individual beads (Fallesen et al. 2010). Unbound beads quickly left the region of interest with the application of a magnetic force. Images of the microtubules and beads were generated by a 60× water immersion objective and a rhodamine fluorescence cube. Images were digitized by a cooled charge-coupled device (CCD) camera (4742-95-12ER; Hamamatsu, Japan). The average length of microtubules was determined by using ImageJ software (http://rsbweb.nih.gov/ij/).

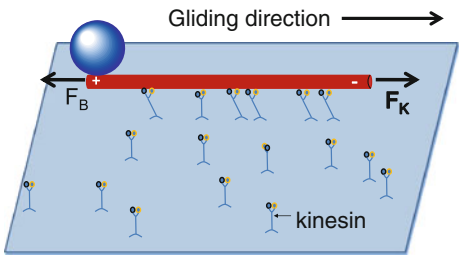

Fig. 1 Schematic of the gliding assay (*color*). Kinesin molecules were attached to the surface by their tails. The heads of the kinesins walked towards the (+) end of the microtubule, applying force F_K to the microtubule. As a result of this force, the (−) end of the microtubule moved in the "Gliding direction" shown at the top of the figure. An M270 magnetic bead (*blue*) is shown attached to the (+) end of the microtubule. When a magnetic field and field gradient were turned on, the bead applied force F_B to the microtubule. The direction of this force was opposite to the direction of F_K

To prevent detachment of the magnetic bead from the microtubule by a high force loading rate when the magnet was turned on to a desired current I^*, the current was increased in 10 smaller steps of $I^*/10$ over 120 ms. This kept the loading rate at 300 pN/s or less. At this loading rate, beads did not detach from the microtubules. This was expected, since the threshold for biotin–streptavidin bond rupture is >50 pN at this loading rate (Pincet and Husson 2005), whereas the maximum force exerted on a bead was 16 pN. Gradual application of current also reduced electrical and mechanical transients in the magnet.

The current was switched from 0 to I^* or I^* to 0 every 45 frames, or 5.42 s with one frame used for gradual turn-on and one frame used for turn-off. The same value of I^* was applied one, two or three times per experimental session, with two, three or four control segments ($I = 0$) in between. Figure 2 shows an experiment with one experimental session ($I^* = 4$ A) and two flanking control sessions ($I = 0$ A).

Determination of the distance between motors attached to a gliding microtubule

The average distance between kinesins was determined in experiments described elsewhere (Fallesen et al. 2011). For those experiments, microtubules were labeled with M270 beads, as described above. Kinesin gliding assays were carried out while a 4–19 pN transverse magnetic force was applied to the bead. This transverse force caused the

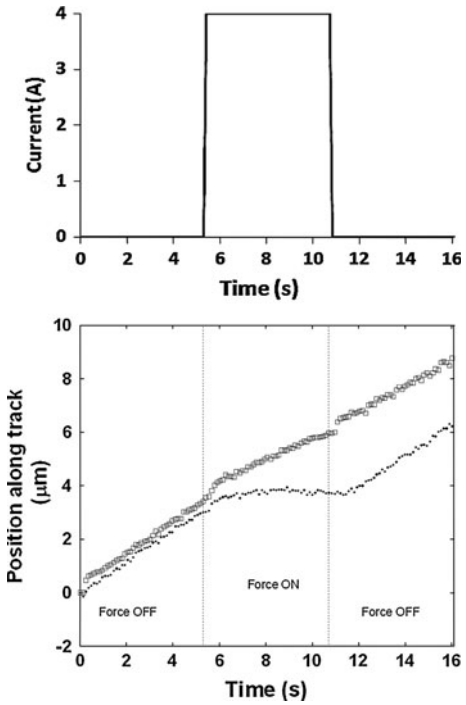

Fig. 2 *Top* time sequence of the magnet current in an experiment. *Bottom* position of the two microtubules as a function of time in response to the current protocol in the top graph. *Filled diamonds* short microtubule ($L = 5.5$ μm). The magnetic force (11.9 pN) was sufficient to bring the microtubule to a halt. Upon removal of the magnetic force, the microtubule resumed its prior motion. *Open square* long microtubule ($L = 10.9$ μm). The magnetic force (11.9 pN) slowed the microtubule down, but did not stop it

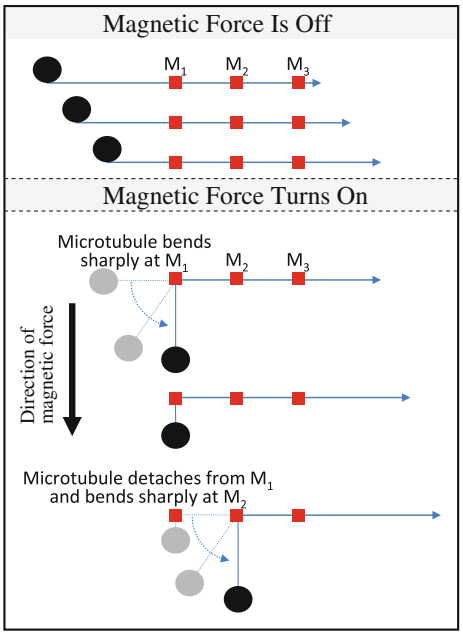

Fig. 3 Diagram of our method for determining the distance between motors (Fallesen et al. 2011). *Black filled circle* magnetic bead, *red filled square* kinesin molecule, *solid blue line* microtubule. The same microtubule is shown at six different times, starting at the top and displaced downward with time for clarity. It is attached to the surface by three motors, designated M_1, M_2, and M_3. The magnetic field is off for the first three time points, so the motors propel to the right both the microtubule leading end and the bead at the trailing (+) end. The transverse magnetic field is then turned on at timepoint 4, causing the bead to move down and revealing the location of M_1 by a sharp bend in the microtubule. At timepoint 5, the motors continue to push the microtubule leading end to the right while the bead is pulled upward. At the last timepoint shown, the microtubule unbinds from M_1 and the bead moves downward until arrested by the next attachment point, M_2. The location of M_2 is revealed by the sharp bend in the microtubule at a new location on the glass surface

normally stiff microtubule to bend sharply by approximately 90° at the nearest motor attaching the microtubule to the surface, as shown diagrammatically in Fig. 3. Meanwhile, the remainder of the microtubule continued to glide in its original direction. After 0.5–2 s, while the magnet continued to apply a transverse force to the bead, the trailing end of the microtubule suddenly detached from M_1. The second attachment point, labeled M_2 in Fig. 3, then revealed itself. The distance between M_1 and M_2 is called d. The average value of d was determined for the same kinesin concentrations used in the current study. The measured values of $\langle d \rangle$ were between 1.7 and 4.0 μm for our kinesin concentrations. Microtubules were prepared for the current study in the same way as for the determination of $\langle d \rangle$, and the two studies were carried out concurrently, so the length distributions are expected to be similar.

Image processing and data analysis

The motion of the tip of a kinesin-driven microtubule from one frame to the next was determined by digital video processing. We used a normalized cross-correlation algorithm (Forstner 1994, Matrox Odyssey Native Language or Matrox MIL 8.0 software) to localize microtubules with subpixel precision. Localization was enhanced by the use of speckled microtubules (Chisena et al. 2007). The velocity of the leading end of the microtubule was independent of the orientation of the microtubule with respect to the direction of the magnetic force. In the event of an opposing force, the tip velocity changes regardless of the direction of travel, as the microtubule acts as a "rope" being pulled opposite to the kinesin driving force by the constant opposing magnetic force. Gliding microtubules were selected for analysis based on length and the gliding angle relative to the direction of force. Only microtubules gliding within ±15° of antiparallel to the opposing force were used for analysis (Fig. 4). For these microtubules, the component of the force parallel to the microtubule axis was between 97% and 100% of the applied force.

The tracking program produced sets of data $\{x,y,t\}$ giving the position (x,y) of the microtubule on the kinesin-coated surface of the capillary tube at each time t during a

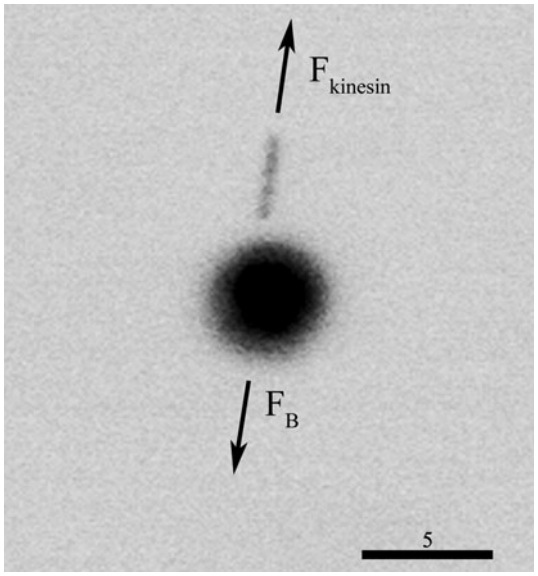

Fig. 4 Kinesin-driven microtubule moving against an opposing magnetic force F_B. The *black sphere* in the center is the M270 superparamagnetic bead. The *straight line* above the bead is the fluorescently labeled section of the microtubule. The bead is connected to the microtubule by a biotin-labeled section of the microtubule, which cannot be seen in this image but is obvious in the video sequence, which shows the bead and the fluorescent section of the microtubule moving at the same speed. The microtubule is moving toward the top of the figure. *Scale bar* 5 μm

"current on" or "current off" experimental session (Fig. 2). Each session lasted 45 frames (5.4 s).

The velocity $v(t)$ of the microtubule along its path was determined from $\{x,y,t\}$ as follows. First, the $\{x,y,t\}$ data were transformed into a new data set $\{x'',y'',t\}$ in which x'' was parallel to the path of the microtubule and y'' was perpendicular to that path [see Appendix for details]. A plot of y'' against t was dominated by high-frequency changes with average value of zero. We assumed y'' to be noise and ignored its contribution to v. A plot of x'' against t showed the translation of the microtubule along its path. Although this plot also had high-frequency noise, its relative value was small compared with the overall translation.

The velocity $v(t)$ could be computed numerically as $\frac{x''(t+\Delta t)-x''(t)}{\Delta t}$; however, with $\Delta t = 1$ frame, this produced a noisy plot of v against t. Inspection of a plot of x'' against t suggested that v was often constant for 5–15 frames, then switched to a new constant velocity, etc. This suggested that smoothing the x'' versus t plot by increasing Δt would smooth away useful information. To determine the times at which v changed and the value of the velocity while it was constant, we carried out a global fit of one to seven linked straight lines to the 45 data points in each $\{x'',t\}$ dataset, using the MATLAB function *fmincon* (Hill et al. 2004). For N_{seg} segments, there were $2N_{seg}$ parameters to fit: N_{seg} slopes, $N_{seg} - 1$ values of time where switches occurred, and one constant to fix the starting point. To decide whether one, two, three, up to seven segments best fitted the data, the reduced χ^2 value was calculated for each of the seven cases. The fit with the lowest reduced χ^2 value was taken as the best fit. Events for which the lowest χ^2 exceeded 6 were excluded from further analysis (Bevington 1969). This removed about 7% of the data. Rare segments with velocities higher than 1,500 nm/s were also excluded. Further details on the experiments and methods of data analysis can be found in the dissertation of Fallesen (2010).

Results

Average velocity

The average velocity $\langle v \rangle$ of microtubules for different values of magnetic force was defined as the weighted average of the segment velocities $\langle v \rangle = \sum_i w_i v_i / \sum_i w_i$, where w_i is the number of frames in segment i. Values of $\langle v \rangle$ for microtubules with attached bead are given in Table 1 for opposing magnetic force F_B ranging from 0 to 31 pN. When the magnetic force was zero, the average velocity was 600–675 nm/s, typical of "no-load" motility assays for multiple kinesin-1 motors. However, when the opposing magnetic force increased to 31 pN, the average velocity decreased substantially, to 220 nm/s. The data in Table 1 were acquired with three different kinesin concentrations and with microtubules of various lengths, so the number of motors pulling a microtubule was not the same for all rows in Table 1.

Average velocity scaled by the number of motors

To account for the expected effect of microtubule length and kinesin concentration on the velocity, we scaled the opposing force F_B by the average number of motors, $\langle n \rangle$ at that current. To obtain $\langle n \rangle$ we assumed that n was directly proportional to the microtubule length L for given kinesin concentration. To account for the effects of kinesin concentration, we used the results of a new method for determining the average distance $\langle d \rangle$ between the motors attached to a microtubule (Fallesen et al. 2011). The values of $\langle d \rangle$, which account for the effects of differing kinesin concentrations used in this paper, are given in Table 1. They varied between 1.7 and 4.0 μm. Knowing $\langle L \rangle$ and $\langle d \rangle$, $\langle n \rangle$ was determined from the relation

$$\langle n \rangle = \langle L \rangle / \langle d \rangle. \quad (2)$$

The resultant values of $\langle n \rangle$ were between 2.6 and 6.9 motors per microtubule for the kinesin concentrations and microtubule lengths used in this work. Finally, knowing

Table 1 Magnetic force, average velocity, and number of motors

F_B (pN)	n_{exp}	[KHC] (μg/mL)	$\langle v \rangle$ (nm/s)	$\langle d \rangle$ (μm)	$\langle L \rangle$ (μm)	$\langle n \rangle$	$F_B/\langle n \rangle$ (pN)
0	72		600–675				0
4	6	1.5	630	4.0 ± 0.5 ($N = 30$)	26.0	6.6	0.61
5.9	10	8.3	590	1.7 ± 0.2 ($N = 20$)	11.5	6.9	0.85
9.1	10	3.9	340	2.4 ± 0.1 ($N = 154$)	6.3	2.6	3.50
11.9	17	3.9	440	2.4 ± 0.1 ($N = 154$)	7.7	3.2	3.75
15.7	20	8.3	470	1.7 ± 0.2 ($N = 20$)	10.2	6.1	2.55
31.4	9	3.9	220	2.4 ± 0.1 ($N = 154$)	15.6	6.5	4.70

Columns: F_B, magnetic force; n_{exp}, number of experiments; [KHC], injected concentration of kinesin; $\langle v \rangle$, average velocity; $\langle d \rangle$, average distance between kinesins with number of measurements, N, in parentheses (Fallesen et al. 2011); $\langle L \rangle$, average length of microtubules; $\langle n \rangle$, average number of motors attached to the microtubules; $F_B/\langle n \rangle$, magnetic force per motor

$\langle n \rangle$, we computed $F/\langle n \rangle$, the magnetic force per motor. The values of $\langle d \rangle$, $\langle L \rangle$, $\langle n \rangle$, and $F/\langle n \rangle$ are given in Table 1.

A plot of average velocity against $F/\langle n \rangle$ is shown in Fig. 5.

The uncertainties in $F/\langle n \rangle$ were calculated by standard propagation of error methods from the uncertainties in F, $\langle d \rangle$, and $\langle L \rangle$. The error in F arose from variations in bead size and calibration of the magnet. The uncertainties in $\langle d \rangle$ are SEM of experiments; the number of experiments is given in Table 1, column for $\langle d \rangle$ (Fallesen et al. 2011). The uncertainty in microtubule length was estimated to be 0.25 μm, approximately two pixels.

Velocity distributions

The distributions of microtubule velocity for various values of the magnetic force F_B per motor were determined by kernel density smoothing (Silverman 1986) of the measured velocities. Gaussian kernels with width in the range 0.035–0.115 μm/s were tested. From visual inspection, a kernel width of 0.060 μm/s gave the best smoothing for the whole data set. The results are shown in Fig. 6.

The velocity distributions have at least two modes. For $F/\langle n \rangle = 0$ pN, the major mode was centered at 650 nm. As $F/\langle n \rangle$ increased, this peak decreased in amplitude and shifted to smaller values of v. A second mode centered at

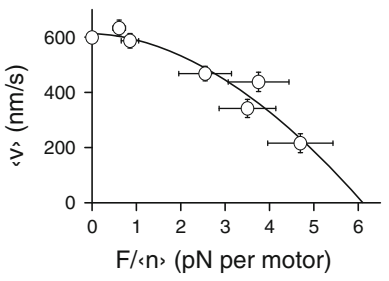

Fig. 5 The average velocity $\langle v \rangle$ of gliding microtubules as a function of magnetic force F_B scaled by the average number of motors. The line is a least-squares fit of Eq. 1 to the data. The best-fit parameters were $v_0 = 610 \pm 50$ nm/s, $F_s = 6.1 \pm 0.7$ pN, and curvature index $w = 1.8 \pm 0.4$. Uncertainties in velocity are SEM of measured values. Uncertainties in $F/\langle n \rangle$ are discussed in the text

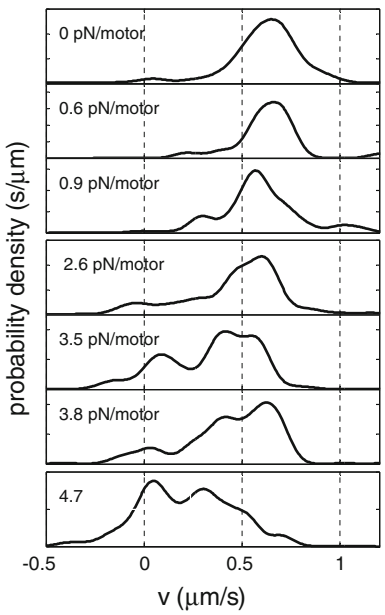

Fig. 6 Velocity distributions for values of $F/\langle n \rangle$ between 0 and 4.7 pN/motor. The distributions were obtained by kernel density smoothing, using a Gaussian kernel of width 0.060 μm/s

$v = 0$ nm/s was visible in almost all of the velocity distributions and grew in amplitude as $F/\langle n \rangle$ increased. At $F/\langle n \rangle = 4.7$ pN/motor, the mode at $v = 0$ was the dominant mode. Several other modes appeared between 0 and 650 nm/s as $F/\langle n \rangle$ increased, but these were poorly resolved.

Discussion

In this work, we applied a force of 4–31 pN to a microtubule during a gliding assay for full-length *Drosophila* kinesin motors. The force was created by attaching a 2.8-μm superparamagnetic bead to the trailing end of the microtubule, then placing the bead in a specially built electromagnet with a spatially uniform field gradient (Fallesen et al. 2010). The available force range extended to 31 pN, well beyond the 5–7 pN stall force for a single motor.

Attachment of a magnetic bead to the (+) end of the microtubule was accomplished with a biotin–streptavidin linkage. Microtubules with biotin-labeled (+) ends were prepared by taking advantage of the difference in polymerization rates at the two ends, and commercially available streptavidin-coated magnetic beads with small size variance. We used the same method previously to attach nonmagnetic beads to the (+) ends of microtubules (Gagliano et al. 2010).

When our movies of the microtubule gliding motion were analyzed by an image-processing program, it became clear that the microtubules did not move at constant velocity or at a constantly changing velocity even though the applied force was constant. Rather, the velocity was constant for 1–3 s, and then changed abruptly to a new constant velocity for a few seconds, etc. as the microtubule glided over the surface.

To understand these velocities within the framework of the known properties of single motors, we plotted the average velocity against the opposing force scaled by the average number of motors $\langle n \rangle$. We evaluated $\langle n \rangle$ from the average microtubule length $\langle L \rangle$ and the average distance $\langle d \rangle$ between motors. The value of $\langle n \rangle$ in our assays was 2–7. Knowing $\langle n \rangle$, we scaled the applied force by $\langle n \rangle$. The plot of v against $F/\langle n \rangle$, given in Fig. 5, fitted the equation $v = v_0\left[1 - \left(\frac{F/\langle n \rangle}{F_s}\right)^w\right]$ with $v_0 = 610 \pm 50$ nm/s, $F_s = 6.1 \pm 0.7$ pN, and $w = 1.8 \pm 0.4$. Data for *single* squid kinesin motors at saturating [ATP] (Visscher et al. 1999) fit the same equation with $v_0 = 800 \pm 50$ nm/s, $F_s = 7.0 \pm 0.3$ pN, and $w = 2.5 \pm 0.4$. The similarity of the parameters suggests that multiple motors act independently and share the load in gliding assays under our conditions.

The determination of $\langle n \rangle$ is critical to our results. Our method works well at low kinesin concentrations, for which d is a few microns. However, our method is destructive to the sample, requires specialized apparatus, and is likely to be difficult to apply at higher kinesin concentrations, because d will then be too small to measure easily by optical microscopy. There remains a need for a simple, nondestructive way to measure the number of active motors over a broad range of motor densities. We note that labeling the motors with green fluorescent protein (GFP) or another fluorophore might permit motors to be located on the surface more easily but would not distinguish between functional and nonfunctional motors. The surface density σ of functional kinesins adsorbed to the chamber walls for gliding assays can be determined from the rate at which microtubules bind to the glass surface of the assay chamber (Howard et al. 1989; Katira et al. 2007). However, this method does not directly measure the number of motors attaching a microtubule to the surface. Our method reveals the attachment points of the moving microtubule. Each attachment point is assumed to mark a single, functional motor.

The distribution of velocities changed under load (Fig. 6). At small load, the distribution was largely in a single mode centered at approximately 650 nm/s. However, as the opposing force increased, the amplitude of this mode grew smaller and its center velocity decreased. In addition, a new mode centered near 0 nm/s became significant with increasing load. We note that, although the center of this mode was at 0 nm/s or slightly positive, there was significant probability for negative velocities, even though the only motor present was kinesin-1. Additional modes occurred between the 650 nm/s mode and the $v = 0$ nm/s mode, but their sizes and locations could not be evaluated with confidence. The width of the 650 nm/s mode was 120 nm/s. Although kernel smoothing broadens each data point to a Gaussian of width 60 nm/s, the observed width was significantly larger.

The changes in the observed velocity distributions with external force (Fig. 6) are similar to the changes predicted by the model of Klumpp and Lipowsky (2005). This supports the view that the observed width of each mode and the presence of several modes when the force increases may both arise from changes in the number of bound kinesin motors. In a gliding assay, n increases whenever a new motor becomes accessible at the leading end of the microtubule, and n decreases whenever the trailing end of the microtubule leaves a previously bound motor behind. In addition, "internal" motors can bind, unbind, and rebind many times, because the stiff microtubule remains near the motor. Such internal processes are central to the Klumpp and Lipowsky (2005) and Kunwar and Mogilner (2010) models of multimotor bead assays.

In the Korn model, the velocity distributions predicted for 1–4 active motors in bead assays are single Gaussians. This prediction is not supported by the observed velocity distributions for our gliding assays (Fig. 6). This discrepancy might in part arise from differences between bead and gliding assays. From single-motor experiments, the binding rate π for one motor has been estimated at 5/s, while the unbinding rate ε has been estimated at 1/s (Klumpp and Lipowsky 2005). The effective unbinding rate ε_n for n motors under load F is given by $\varepsilon_n = n\varepsilon \exp\left(\frac{F}{nF_d}\right)$, where the detachment force $F_d \approx 3$ pN. For $n = 6$ and $F/n = 4$ pN, about the middle of our experimental range, $\varepsilon_n \approx 23\ s^{-1}$. This is faster than the frame rate of our camera. This suggests that internal changes in n occur too rapidly for our current experimental setup to detect.

The rates for changes in n at the leading and trailing ends of the microtubule can be estimated from the velocity of the microtubule and the distance between active motors, both of which are known (Table 1). For $d = 2$ μm and $v = 0.4$ μm/s, typical for our experiments, the rate v/d is 0.2/s, about one change in n every 5 s. Such slow processes would be observable in our experiments. This suggests that the discrete changes in velocity which we observe arise in part from changes in motor number at the leading and trailing ends of the microtubule.

How do our results map onto the results of other motility assays? In a gliding assay, Leduc et al. (2007) detect the individual steps of microtubules transported by two kinesin-1 motors in the absence of significant load. They find that microtubules propelled by two motors often take 4-nm steps, half the step size of single motors. This shows that the steps of the two motors are not coordinated if pulling against negligible load.

Beeg et al. (2008) measure the velocities and run lengths of kinesin-coated beads along microtubules in vitro. The surface density of kinesin bound to the bead is determined by a novel optical method, which shows that beads carry 1–6 motors. The binding rate of beads to microtubules, as well as the run lengths, increase with increasing kinesin surface density, but the average velocity is independent of the kinesin density. We also observed that velocity was independent of the number of kinesin motors when the magnet current (opposing force) was zero; this was the control segment of our experiments (Fig. 2). However, when the magnet current was turned on, providing a force of 2–5 pN per motor, the velocity depended on the number of motors (Figs. 2, 5).

A similar pattern occurs during gliding assays of kinesin in a viscoelastic medium if some of the microtubules have an attached bead while others do not (Gagliano et al. 2010). Microtubules without a bead experience negligible drag and move at 700 nm/s regardless of microtubule length, whereas microtubules with a bead exhibit length-dependent velocity: 2-μm microtubules move at 150 nm/s, whereas 30-μm microtubules move at 700 nm/s, because the longer microtubule is moved by many more motors.

Some caution may be appropriate when applying insights gleaned from microtubule gliding assays and bead assays to vesicle transport in vivo. In vitro, the tails of the motors are attached to fixed positions on the glass surface or bead. However, in vivo, motor tails may be free to move on the vesicle surface while remaining bound. Experiments with membrane nanotubes show that the motors accumulate at the tip of the tube (Leduc et al. 2004). Whether such accumulation occurs in cells, and whether it helps or hinders vesicle movement in vivo, remains an open question.

In summary, this study showed that 2–7 kinesin-1 motors were able to move a microtubule at velocities of 200–600 nm/s against an external magnetic force of 4–31 pN. When the force was scaled by the number of motors, the average velocity for multiple motors varied with $F/\langle n \rangle$ in a manner quantitatively similar to the well-studied F-v behavior curves for a single motor. This showed that a minimal load-sharing model was sufficient to describe the effects of multiple motors on microtubule velocity during gliding assays.

Acknowledgments We thank J. Howard for providing plasmid pPK113 for kinesin-1, Jason Gagliano for assistance in the preparation of kinesin, and Matt Steen for assistance with Odyssey software. We are grateful for helpful suggestions from the reviewers. Support from NIH grant R15 NS053493 (G.H.) and Wake Forest University funds (J.C.M.) is gratefully acknowledged.

Appendix

Conversion of $\{x,y,t\}$ tracks to $\{x'',y'',t\}$ data for which x'' is parallel to the path of the microtubule and y'' is perpendicular to that path.

Consider a microtubule traveling at constant velocity in a straight path, $x = x_0 + v_x t$, $y = y_0 + v_y t$, with v_x and v_y independent of t.

Step 1. Translocate the (x,y,t) frame to a new coordinate frame (x',y',t) in which the microtubule starts at (0,0,0) with equations $x' = x - x_0$, $y' = y - y_0$. In the $x'y'$ plane, $y' = (v_y/v_x)x'$, a straight line through the origin.

Step 2. Rotate the (x',y') coordinate system by angle $\theta = \tan^{-1}(v_y/v_x)$ to new coordinates (x'',y''): $\begin{bmatrix} x'' \\ y'' \end{bmatrix} = \begin{bmatrix} \cos(\theta) & \sin(\theta) \\ -\sin(\theta) & \cos(\theta) \end{bmatrix} \begin{bmatrix} x' \\ y' \end{bmatrix}$.

In the (x'',y'') coordinate system, $x'' = \left(\sqrt{v_x^2 + v_y^2}\right)t = vt$ and $y'' = 0$. Thus, the slope $\frac{dy''}{dt}$ equals the velocity of the particle.

For a microtubule traveling along a curved path, v_x and v_y are functions of t, so $\theta = \tan^{-1}(v_y/v_x)$ is also a function of t. We determined $\theta(t)$ from the smoothed value of dy/dx. Steps 1 and 2 were then applied to data points 1 and 2. This done, steps 1 and 2 were applied to points 2 and 3, etc. (This is easy in MATLAB.) In that (x'',y'',t) coordinate system, $y''(t) = 0 + \text{noise}$, whereas $x''(t) = vt + \text{noise}$. We tested the algorithm carefully with synthetic data, i.e., data sets $\{x,y,t\}$ constructed with known values of v_x and v_y, plus Gaussian noise.

References

Beeg J, Klumpp S, Dimova R, Garcia RS, Unger E (2008) Transport of beads by several kinesin motors. Biophys J 94:532–541

Bevington PR (1969) Data reduction and error analysis for the physical sciences. McGraw-Hill, New York

Bieling P, Telley IA, Piehler J, Surrey T (2008) Processive kinesins require loose mechanical coupling for efficient collective motility. EMBO Reports 1–7

Block SM, Goldstein LSB, Schnapp BJ (1990) Bead movement by single kinesin molecules studied with optical tweezers. Nature 348:348–352

Chisena EN, Wall RA, Macosko JC, Holzwarth GM (2007) Speckled microtubules improve tracking in motor-protein gliding assays. Phys Biol 7:10–15

Coppin CM, Pierce DW, Hsu L, Vale RD (1997) The load dependence of kinesin's mechanical cycle. Proc Natl Acad Sci USA 94:8539–8544

Coy DL, Wagenbach M, Howard J (1999) Kinesin takes one 8-nm step for each ATP that it hydrolyzes. J Biol Chem 274: 3667–3671

Fallesen TL (2010) Kinesin-microtubule interactions during gliding assays under magnetic force physics. Wake Forest University, Winston-Salem, pp 193, http://hdl.handle.net/10339/30429

Fallesen TL, Hill DB, Steen M, Macosko JC, Bonin KGH (2010) Magnet polepiece design for uniform magnetic force on superparamagnetic beads. Rev Sci Inst 81:074303

Fallesen TL, Macosko JC, Holzwarth G (2011) Measuring the number and spacing of molecular motors propelling a gliding microtubule. Phys Rev E 83:011918, http://link.aps.org/doi/10.1103/PhysRevE.83.011918

Forstner W (1994) Image matching. In: Haralick RM, Shapiro LG (eds) Computer and robot vision, vol 2. Addison-Wesley, Reading, MA, pp 289–378

Gagliano J, Walb M, Blaker B, Macosko JC, Holzwarth G (2010) Kinesin velocity increases with the number of motors pulling against viscoelastic drag. Eur Biophys J 39:801–813

Gibbons F, Chauwin J-F, Desposito M, Jose JV (2001) A dynamic model of kinesin-microtublue motility assays. Biophys J 80:2515–2526

Hill DB, Plaza MJ, Bonin KD, Holzwarth G (2004) Fast Vesicle Transport in PC12 Neurites: velocities and forces. Eur Biophys J 33:623–632

Hirokawa N, Noda Y, Tanaka Y, Niwa S (2009) Kinesin superfamily motor proteins and intracellullar transport. Nat Rev Mol Cell Biol 10:662–696

Howard J (2001) Mechanics of motor proteins and the cytoskeleton. Sinauer Associates, Sunderland, MA

Howard J, Hudspeth AJ, Vale RD (1989) Movement of microtubules by single kinesin molecules. Nature 342:154–158

Hunt AJ, Gittes F, Howard J (1994) The force exerted by a single kinesin molecule against a viscous load. Biophys J 67:766–781

Jamison DK, Driver JW, Rogers AR, Constantinou PE, Diehl MR (2010) Two kinesins transport cargo primarily via the action of one motor: implications for intracellular transport. Biophys J 99:2967–2977

Katira P, Agarwal A, Fischer T, Chen H-Y, Jiang X, Lahann J, Hess H (2007) Quantifying the performance of protein-resisting surfaces at ultra-low protein coverages using kinesin motor proteins as probes. Adv Mater 19:3171–3176

Klumpp S, Lipowsky R (2005) Cooperative cargo transport by several molecular motors. Proc Natl Acad Sci USA 102:17284–17289

Kojima H, Muto E, Higuchi H, Yanagida T (1997) Mechanics of single kinesin molecules measured by optical trapping nanometry. Biophys J 73:2012–2022

Korn CB, Klumpp S, Lipowsky R, Schwarz US (2009) Stochastic simulations of cargo transport by processive molecular motors. J Chem Phys 131:245107

Kunwar A, Mogilner A (2010) Robust transport by multiple motors with nonlinear force-velocity relations and stochastic load sharing. Phys Biol 7:016012

Leduc C, Campas O, Zeldovich KB, Roux A, Jolimaitre P, Borel-Bonnet L, Goud B, Joanny J-F, Prost J (2004) Cooperative extraction of membrane nanotubes by molecular motors. Proc Natl Acad Sci USA 101:17096–17101

Leduc C, Ruhnow F, Howard J, Diez S (2007) Detection of fractional steps in cargo movement by the collective operation of kinesin-1 motors. Proc Natl Acad Sci USA 104:10847–10852

Meyhöfer E, Howard J (1995) The force generated by a single kinesin molecule against an elastic load. Proc Natl Acad Sci USA 92:574–578

Nan X, Sims PA, Xie XS (2008) Organelle tracking in a living cell with microsecond time resolution and nanometer spatial precision. ChemPhysChem 2008:707–712

Pincet F, Husson J (2005) The solution to the streptavidin-biotin paradox: the influence of history on the strength of single molecular bonds. Biophys J 89:4374–4381

Shtridelman Y, Holzwarth GM, Bauer CT, Gassman NR, DeWitt DA, Macosko JC (2009) In vivo multimotor force-velocity curves by tracking and sizing sub-diffraction limited vesicles. Cel Mol Bioeng 2:190–199

Shubeita GT, Tran SL, Xu J, Vershinin M, Cermelli S, Cotton SL, Welte MA, Gross SP (2008) Consequences of motor copy number on the intracellular transport of kinesin-1-driven lipid droplets. Cell 135:1098–1107

Silverman BW (1986) Density estimation for statistics and data analysis, 1st edn. Chapman and Hall, London

Vale RD, Malik F, Brown D (1992) Directional instability of microtubule transport in the presence of kinesin and dynein, two opposite polarity motor proteins. J Cell Biol 119:1589–1596

Vershinin M, Carter BC, Razafsky DS, King SJ, Gross SP (2007) Multiple-motor based transport and its regulation by Tau. Proc Natl Acad Sci USA 104:87–92

Visscher K, Schnitzer MJ, Block SM (1999) Single kinesin molecules studied with a molecular force clamp. Nature 400:184–189

Watanabe TM, Higuchi H (2007) Stepwise movements in vesicle transport of HER2 by motor proteins in living cells. Biophys J 92:4109–4120

Welte MA, Gross S, Postner M, Block S, Wieschaus E (1998) Developmental regulation of vesicle transport in Drosophila embryos: forces and kinetics. Cell 92:547–557

Yildiz A, Tomishige M, Vale RD, Selvin PR (2004) Kinesin walks hand-over-hand. Science 303:676–678